
Three-dimensional Thermography Mapping for Mobile Rescue Robots

Keiji NAGATANI¹, Kazuki OTAKE¹, and Kazuya Yoshida¹

Tohoku University

Summary. In urban search and rescue situations, a 3D map obtained using a 3D range sensor mounted on a rescue robot is very useful in determining a rescue crew's strategy. Furthermore, thermal images captured by an infrared camera enable rescue workers to effectively locate victims. The objective of this study is to develop a 3D thermography mapping system using a 3D map and thermal images; this system is to be mounted on a tele-operated (or autonomous) mobile rescue robot. The proposed system enables the operator to understand the shape and temperature of the disaster environment at a glance. To realize the proposed system, we developed a 3D laser scanner comprising a 2D laser scanner, DC motor, and rotary electrical connector. We used a conventional infrared camera to capture thermal images. To develop a 3D thermography map, we integrated the thermal images and the 3D range data using a geometric method. Furthermore, to enable fast exploration, we propose a method for continuous thermography mapping while the robot is in motion. This method can be realized by synchronizing the robot's position and orientation with the obtained sensing data. The performance of the system was experimentally evaluated in real-world conditions. In addition, we extended the proposed method by introducing an improved iterative closest point (ICP) scan matching algorithm called thermo-ICP, which uses temperature information. In this paper, we report development of (1) a 3D thermography mapping system and (2) a scan matching method using temperature information.

Key words: Search and Rescue, 3D Thermography Mapping

1 Introduction

Recently, there has been a growing demand for preliminary robotic investigation in urban search and rescue missions conducted at sites affected by disasters such as earthquakes or terror attacks. For this purpose, search and rescue robots are being developed by a number of institutes [1], particularly in Japan [2] [3].

The important functions of rescue robots are to search for victims and to gather environmental information for planning rescue operations. Useful information for the former function constitutes biological signals such as

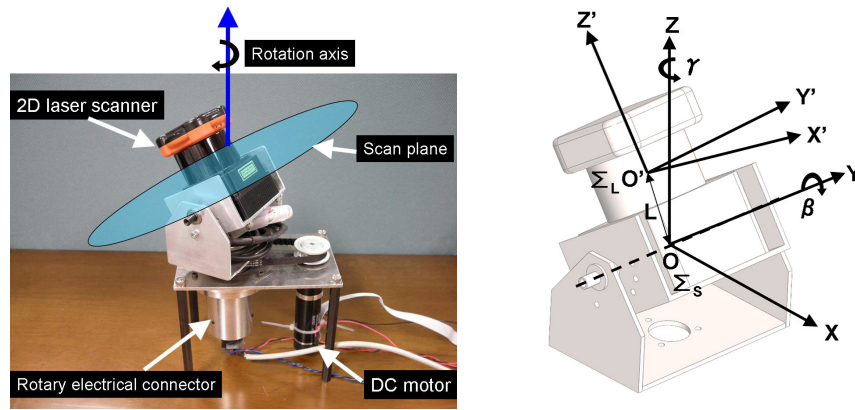


Fig. 1. 3D scanner (left) and coordinate system (right)

body temperature and carbon dioxide, whereas that for the latter function continues images, three-dimensional (3D) shapes [4], temperature, and gas concentration in the target environment. In both cases, infrared cameras are indispensable, particularly in dark conditions. In the 2011 RoboCupRescue competition [5], such cameras mounted on rescue robots were widely used for identifying simulated victims which have heat sources. However, the two-dimensional (2D) information captured by the camera makes it difficult for rescue crews to deduce 3D structures.

Therefore, in this study, we propose a sensor fusion method to integrate a 3D-map captured by a 3D range scanner with infrared images captured by an infrared camera, to construct a 3D thermography map. The integration of a 3D map and color images has been investigated in several studies [6] [7] [8]. Recently, some studies on 3D thermography mapping were conducted [9] [10]. However, to the best of our knowledge, this technology has not been applied to rescue robots thus far. The proposed method enables rapid mapping for rescue scenarios. To realize map building, the robot acquires environmental information while it is in motion. We installed the proposed system on a mobile rescue robot testbed called Kenaf in order to verify the validity of the method.

2 3D range scanner

Conventional commercial 3D range scanners are expensive and bulky. Therefore, we decided to develop a small, light weight 3D range scanner for this study. In general, a 3D range scanner is realized by rotating a conventional 2D laser range scanner. We adopted this method, as described in the following section.

2.1 Hardware

The 3D range scanner that we developed consists of a 2D laser range scanner (UTM-30LX, HOKUYO Co., Ltd.), DC motor (RE25, Maxon Motor), and rotary connector (Model630, Mercotac). A schematic of the scanner is shown in Fig.1 (left).

The 2D scanner is attached to a rotating table at a certain angle, β . Thus, the scanning surface of the 2D scanner is inclined to the rotating surface of the table, so that 3D environment information is obtained by rotating the table [11]. At the rotation axis of the table, we installed a rotary electrical connector that having a mercury contact. Therefore, the table with the 2D scanner can rotate freely without causing the cables to twist. The rotation speed of the table can be increased up to 180 rpm, and frequency 3D range scanning can be performed using this device.

2.2 Geometric model

Here, we introduce the geometric model of the 3D range scanner, as shown in Fig.1 (right). Let us assume that the coordination system \sum_L is attached to the 2D scanner. The origin O' of the coordinate is located at the center of the scanning surface, the x-axis X' corresponds to the front of the scanner, the z-axis Z' is perpendicular to the scanning surface, and the y-axis Y' is defined to satisfy the right-handed coordinate system. The coordination system \sum_S is attached to the 3D range scanner, and the origin O of the coordinate is located at a certain distance above the center of the rotation table. The x-axis X corresponds to the front of the 3D range scanner, the z-axis Z corresponds to the rotational axis of the table, and the y-axis Y is defined to satisfy the right-handed coordinate system. The mounting angle of the 2D scanner is β , and rotational speed of the table is $\dot{\gamma}$. The homogeneous transform matrix ${}^S\mathbf{T}_L$ between \sum_L and \sum_S is expressed by:

$${}^S\mathbf{T}_L = \begin{bmatrix} {}^S\mathbf{R}_L & {}^S\mathbf{t}_L \\ 0 & 1 \end{bmatrix} \quad (1)$$

$${}^S\mathbf{R}_L = \begin{bmatrix} \cos\gamma & -\sin\gamma & 0 \\ \sin\gamma & \cos\gamma & 0 \\ 0 & 0 & 1 \end{bmatrix} \begin{bmatrix} \cos\beta & 0 & \sin\beta \\ 0 & 1 & 0 \\ -\sin\beta & 0 & \cos\beta \end{bmatrix} \quad (2)$$

$${}^S\mathbf{t}_L = {}^S\mathbf{R}_L \begin{bmatrix} 0 \\ 0 \\ L \end{bmatrix} \quad (3)$$

where ${}^S\mathbf{R}_L$ and ${}^S\mathbf{t}_L$ are the rotation and translation matrices of \sum_L relative to \sum_S , and γ and β are rotations around the Z-axis and the Y-axis, respectively. A measured point ${}^L\mathbf{p}$ relative to \sum_L is expressed by:

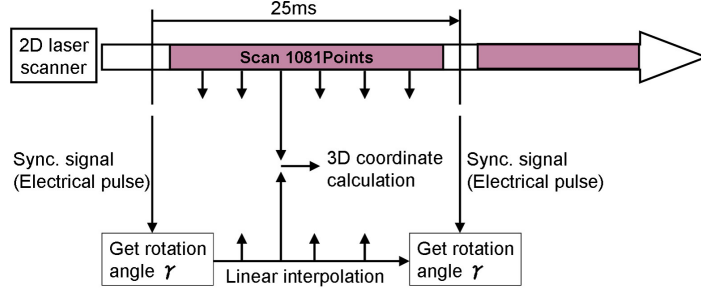


Fig. 2. Conceptual diagram of synchronization

$${}^L\mathbf{p} = \begin{bmatrix} {}^L p_x \\ {}^L p_y \\ {}^L p_z \end{bmatrix} = \begin{bmatrix} r \cos \theta \\ r \sin \theta \\ 0 \end{bmatrix} \quad (4)$$

where r represents the measured distance, and θ represents the scanning angle. Finally, the measured point coordinate ${}^S\mathbf{p}$ relative to Σ_S is

$${}^S\mathbf{p} = {}^S\mathbf{T}_L {}^L\mathbf{p} \quad (5)$$

$$\begin{bmatrix} {}^S p_x \\ {}^S p_y \\ {}^S p_z \end{bmatrix} = \begin{bmatrix} \cos \gamma & -\sin \gamma & 0 \\ \sin \gamma & \cos \gamma & 0 \\ 0 & 0 & 1 \end{bmatrix} \begin{bmatrix} \cos \beta & 0 & \sin \beta \\ 0 & 1 & 0 \\ -\sin \beta & 0 & \cos \beta \end{bmatrix} \begin{bmatrix} r \cos \theta \\ r \sin \theta \\ L \end{bmatrix}. \quad (6)$$

2.3 Control Architecture

To obtain accurate 3D Cartesian coordinates of sensing points ${}^S\mathbf{p}$, synchronization between the scan data and the rotation angle of the table γ is very important. In our control architecture, we use a synchronizing signal from the 2D scanner, a signal of the encoder attached to the motor rotating the table, H8S micro control unit (MCU), and a host PC. Figure 2 shows a conceptual diagram of the synchronization. The 2D scanner sends 1,081 points of measurement data ${}^L\mathbf{p}$ every 25 ms to the host PC. The synchronizing digital signal is also generated by the scanner, and it becomes a trigger for reading the encoder data. We assume that the rotation speed $\dot{\gamma}$ is constant, so that linear interpolation is conducted to obtain γ for each sensory reading.

3 3D Thermography Mapping System

To construct a 3D thermography map, we need a wide-view infrared image. However, the view angle of a conventional infrared camera is typically small. For the purpose of 3D thermography mapping, the camera should be mounted

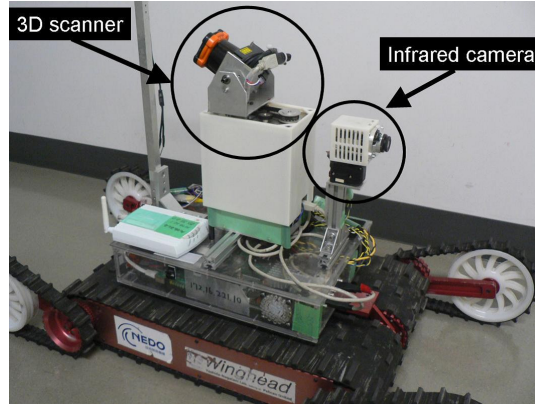


Fig. 3. Kenaf equipped with 3D scanner and infrared camera

on a rotating table. Furthermore, we conducted a calibration of the camera's distortion in order to integrate a 3D range map and infrared images. Finally, we extended the method to provide a moving measurement system for mobile robots, as described in this section.

3.1 Hardware

Ideally, the focal position of the infrared camera and the center of the 3D range scanner should be the same. Practically, this is impossible, and we should ensure that they do not occlude each other. Therefore, we place the infrared camera and the 3D range scanner at different heights, as shown in Fig.3.

We chose infrared camera module HX0830M2, manufactured by NEC Avio infrared technologies Co., Ltd. as our target infrared camera. The pixel number of the camera is 320(H) \times 240(V), and the field of view is 50 $^{\circ}$ \times 37.5 $^{\circ}$. To rotate to which the camera is attached, we chose a smart motor, Dynamixel DX-117, manufactured by ROBOTIS Inc. By using the camera module and rotating the table from -90 $^{\circ}$ to 90 $^{\circ}$, we can obtain a wide infrared image: 50 $^{\circ}$ in the vertical field of view and 217.5 $^{\circ}$ in the horizontal.

3.2 Geometric model

Here, we introduce a method to match a scan point ${}^S\mathbf{p}$ with a pixel in an infrared image. The coordination system of the scanner system is shown in Fig.4 (left). Let us assume that the coordination system \sum_C is attached to a camera. The origin O'' of the coordinate is located at the focal position of the camera, the x-axis X'' corresponds to the optical axis, the z-axis Z'' corresponds to the vertical coordinate of the camera, and the y-axis Y'' is defined to satisfy the right-handed coordinate system. A scan point ${}^C\mathbf{p}$ represented by \sum_C is calculated by

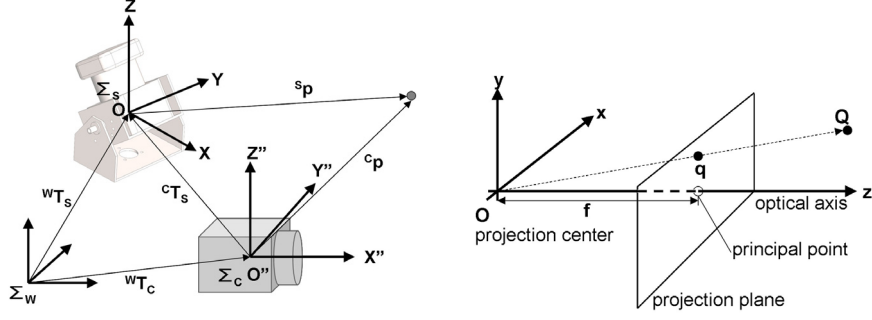


Fig. 4. Coordinate system of thermography mapping system (left) and projection model of the camera (right)

$${}^C \mathbf{p} = {}^C T_S {}^S \mathbf{p}, \quad (7)$$

where ${}^C T_S$ is the homogeneous transform between Σ_S and Σ_C . In fact, the positional relationship ${}^W T_S$ between Σ_S and Σ_W (the world coordinate system) is known, and ${}^W T_C$ between Σ_C and Σ_W is calculated by camera position and camera rotating angle. Therefore, ${}^C T_S$ is obtained by the equation

$${}^C T_S = {}^C T_W {}^W T_S \quad (8)$$

$$= {}^W T_C^{-1} {}^W T_S \quad (9)$$

$$= \begin{bmatrix} {}^W R_C^T & -{}^W R_C^T {}^W T_C \\ 0 & 1 \end{bmatrix} \begin{bmatrix} {}^W R_S & {}^W T_S \\ 0 & 1 \end{bmatrix} \quad (10)$$

$$= \begin{bmatrix} {}^W R_C^T {}^W R_S & {}^W R_C^T ({}^W T_S - {}^W T_C) \\ 0 & 1 \end{bmatrix}. \quad (11)$$

Finally, Equation(7) is represented by

$${}^C \mathbf{p} = \begin{bmatrix} {}^W R_C^T {}^W R_S & {}^W R_C^T ({}^W T_S - {}^W T_C) \\ 0 & 1 \end{bmatrix} {}^S \mathbf{p}. \quad (12)$$

In case of exchanging from Σ_W to the robot coordinate system Σ_{RS} , equation(12) represents a scan point when the robot is motionless. In section 3.4, it will be extended to the scan point model when the robot is moving.

The next step is to obtain the scan point coordinate on the infrared image. Figure 4(right) shows the projection model of the camera. The transform from 3D point $Q = (X, Y, Z)$ to an image point $q = (x, y)$ is conducted by the homogeneous coordination $\hat{q} = (x, y, 1)^T$ and the equation

$$\omega \hat{q} = M Q. \quad (13)$$

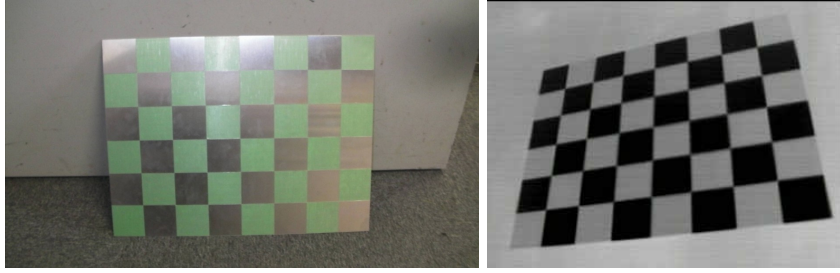


Fig. 5. Developed calibration board (left) and obtained image (right)

$$\mathbf{M} = \begin{bmatrix} f_x & 0 & c_x \\ 0 & f_y & c_y \\ 0 & 0 & 1 \end{bmatrix} \quad (14)$$

where M is the internal parameter matrix of the camera, f_x and f_y represent the focal lengths, and c_x and c_y are the offsets of the projection center.

Equation (13) is satisfied only when there is no lens distortion. Practically, distortion calibration of the infrared camera is required, as shown in the next sub-section.

3.3 Distortion calibration of infrared camera

To obtain the internal and distortion parameters of the infrared camera, we applied Zhang's method [12]. This method requires images of the calibration pattern to be obtained at different locations. In this study, we used an infrared camera; thus, an ingenious method was required to obtain clear calibration patterns. Therefore, we developed a calibration board composed of high-infrared-reflectance aluminum and low-infrared-reflectance masking tape [13], as shown in Fig.5 (left). The size of the board was 300 mm \times 400 mm, and its grid size was 50 mm. Based on the above method, we were able to obtain clear images of the board (see Fig.5(right)) when the surface of the board reflected the sky outside.

3.4 Extension to moving measurement system

To enable rapid map building, we extended the thermography mapping method to a moving measurement system for mobile robots. The method is based on a gyroscope-based 3D odometry system [14].

Let us assume that \sum_{RS} is the robot coordinate system when the scanner captures data, and \sum_{RC} is the robot coordinate system when the camera captures an image. The homogeneous transform matrix ${}^C\mathbf{T}_S$ (to represent \sum_S relative to \sum_C) is decomposed as

$${}^C\mathbf{T}_S = {}^C\mathbf{T}_{RC} {}^{RC}\mathbf{T}_W {}^W\mathbf{T}_{RS} {}^{RS}\mathbf{T}_S, \quad (15)$$

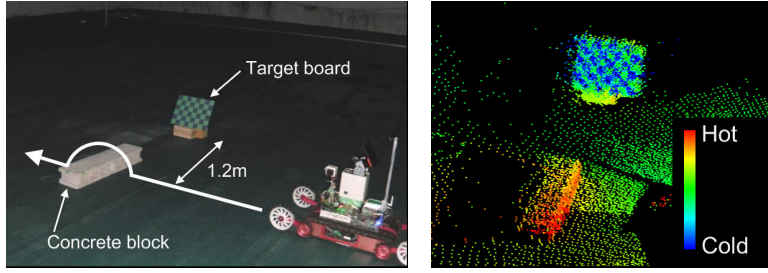


Fig. 6. Setup of the basic experiment (left) and the mapping result (right)

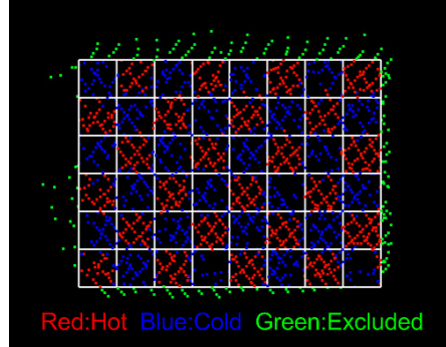


Fig. 7. Binarized thermography map of the target board

where ${}^{RS}\mathbf{T}_S$ is the homogeneous transform matrix that represents the scanner coordinate relative to the robot coordinate, and ${}^{RC}\mathbf{T}_C$ is the homogeneous transform matrix that represents the camera coordinate relative to the robot coordinate. ${}^W\mathbf{T}_{RS}$ and ${}^W\mathbf{T}_{RC}$ are obtained by the 3D odometry system, ${}^C\mathbf{T}_{RC}$ and ${}^{RC}\mathbf{T}_W$ can be calculated from ${}^{RC}\mathbf{T}_C$ and ${}^W\mathbf{T}_{RC}$. Finally, ${}^C\mathbf{p}$ is obtained by Equation (7).

3.5 Synchronization between the scan data and the odometry data

Because the sampling time of the odometer is different from that of the scanner, we applied time stamps to synchronize the scan data and the odometry data. To achieve precise synchronization, we applied a linear interpolation of the odometry data. The details are explained in [14].

3.6 Initial experiment

To evaluate our 3D thermography mapping system, we conducted an initial mapping experiment, as shown in Fig.6. The translation speed of the robot was typically about 4.3 cm/s, and it surmounted a concrete block while it mapped the environment three-dimensionally. The distance from the robot's

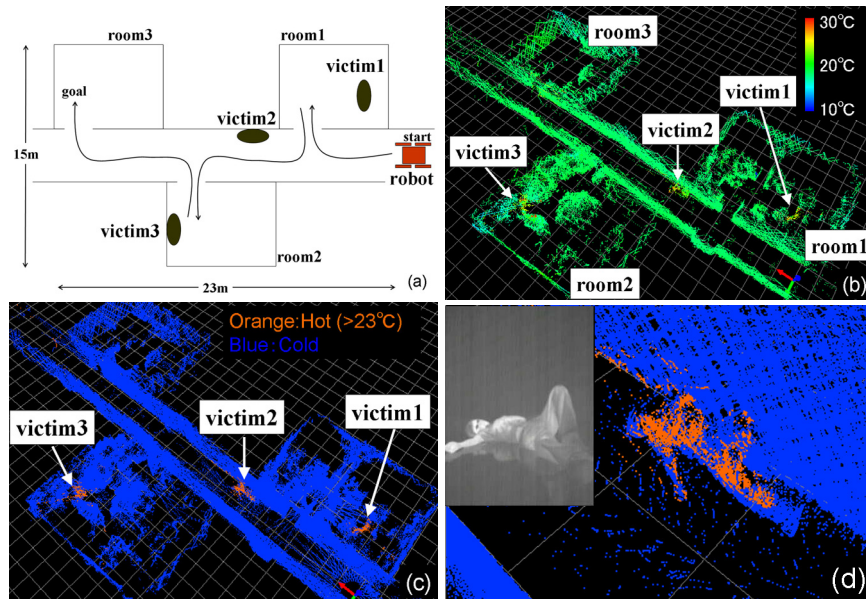


Fig. 8. Experiments in wide area. (a) setup of the experiment, (b) mapping result, (c) binarized mapping result, (d) zoomed-in view of victim 2

path to the target board was 1.2 m. The mounting angle of the 2D scanner, β , was set at 60° , and the rotation speed of the table $\dot{\gamma}$ was set at 6 rpm.

Figure 6(right) shows a thermography mapping result. In this figure, the block and the target calibration board can be seen: the image does not collapse because of the robot's motion.

Figure 7 shows the binarized result of one scan (10 s) while the robot surmounted the blocks. During the motion, the transition vector of the robot is $(x, y, z, \phi_x, \phi_y, \phi_z) = (+164\text{mm}, +4\text{mm}, +15\text{mm}, -0.4\text{deg}, +16.7\text{deg}, +0.5\text{deg})$. In this figure, the white frame represents the ideal boundaries of the lattice, red dots represent high-temperature points, blue dots represent low temperature points, and green dots represent excluded measurement points. The total number of dots in the board was 1,733, and the number of dots assigned correctly was 1,492. Thus, the proportion of dots assigned correctly was 86.1 %. According to the above results, the thermography mapping of the range data was conducted precisely, even if the robot surmounted the block. The errors were attributed to the laser beam being slightly conical in shape, so that the reflection close to the edge of the board returned.

3.7 Experiments in wide area

To evaluate our 3D thermography mapping system, we conducted a wide-area experiment, shown in Fig.8. The target environment is the fourth floor of the

building that houses our laboratories', which includes three rooms connected by a straight corridor, as shown in Fig.8 (a). We located three dummy victims. Figure 8 (b) shows a thermography mapping result, and Fig.8 (c) shows a binarized thermography mapping result. Figure 8 (d) shows a zoomed-in view of victim 2 and a raw infrared image.

Based on the results, the target environment was measured with no distortion, even if it was measured by only a gyroscope-based odometry system, because the robot navigated on a flat surface. Furthermore, we understood that, since it focuses on the detected victims, a binarized map is an effective aid for human operators, as shown in Fig. 8(c).

4 Thermo-ICP (thermography-based iterative closest point) matching method

As an application of the 3D thermography mapping system, we introduce a thermography-based iterative closest point (ICP) matching method, called Thermo-ICP. A conventional ICP-matching method [15] relies on the shape of the environment's features. Therefore, it is difficult to apply the method to an environment that has a small number of geometrical features, such as a long corridor. Some methods use color information for ICP matching; however, such methods are sensitive to lighting conditions. Therefore, in this study, we used temperature information as a feature for ICP matching.

4.1 Temperature-shift according to measurement position

To use temperature data for ICP matching, the target temperature should be the same, regardless of the position from which it is measured.

First, we consider a temperature measurement at a glancing angle θ . Infrared rays emitted from a point source decrease according to the glancing angle θ (Lambert's cosine law) as:

$$I_{\theta} = I_0 \times \cos\theta. \quad (16)$$

On the other hand, the target size D_{θ} increases according to the glancing angle θ :

$$D_{\theta} = D_0 \times \frac{1}{\cos\theta}. \quad (17)$$

Thus, the total amount of infrared rays for each pixel of a camera $I_{\theta}D_{\theta}$ is equal to I_0D_0 .

Practically, an object that has low emissivity of infrared rays has angular dependency. Therefore, it is said that a reasonable measurement angle θ is within $\pm 45^{\circ}$.

Second, we consider the distance from the camera to the measured object. The emitted power of infrared rays is inversely proportionally with the square

of the distance from a heat source. On the other hand, the target size increases proportional to the square of the distance from the heat source. Thus, the total amount of infrared rays for each pixel of a camera is independent of its distance from the heat source. However, in practice, the effect of water vapor or flue dust increases with the distance between the camera and the object.

Accordingly, we used temperature data when the measurement angle θ was within $\pm 45^\circ$, and the distance was not too great for thermo-ICP.

4.2 ICP matching method

ICP matching is a popular method for fitting two sets of shape data based on geometric features. Mobile robots that can reconstruct environmental information and conduct SLAM (simultaneous localization and mapping) are very useful. In this subsection, we would like to introduce a brief description of conventional ICP matching.

In this method, two sets of sensing points are registered in Cartesian coordinates. In each iteration step, the algorithm selects the closest points as correspondences and calculates the rotation matrix \mathbf{R} and the translation matrix \mathbf{t} to minimize the equation

$$E(\mathbf{R}, \mathbf{t}) = \sum_{i=1}^{N_m} \sum_{j=1}^{N_d} \omega_{i,j} \|\mathbf{m}_i - (\mathbf{R}\mathbf{d}_j + \mathbf{t})\|^2, \quad (18)$$

where N_m and N_d are the number of points in the reference data set \mathbf{M} and the matching data set \mathbf{D} , respectively. $\omega_{i,j} = 1$ when \mathbf{m}_i in \mathbf{M} is the closest point to \mathbf{d}_j in \mathbf{D} , and $\omega_{i,j} = 0$ otherwise. Newton's method is typically used for calculating \mathbf{R} and \mathbf{t} in the evaluation function.

4.3 Thermo-ICP matching

Our Thermo-ICP matching uses not only Euclidean distances but also temperature difference to search for corresponding points. The evaluation function of the algorithm uses not only the squared sum of the closest distance, but also the squared difference of thermo-values. Thus, the evaluation function for thermo-ICP is

$$E_T(\mathbf{R}, \mathbf{t}) = \sum_{i=1}^{N_m} \sum_{j=1}^{N_d} \hat{\omega}_{i,j} \left(\|\mathbf{m}_i - (\mathbf{R}\mathbf{d}_j + \mathbf{t})\|^2 + K|h_{mi} - h_{dj}|^2 \right), \quad (19)$$

where K represents a weighting factor of the temperature term. Currently, we don't have any method to determine the value K , instead we set the parameter empirically. h_{mi} is the temperature value of \mathbf{m}_i , and h_{dj} is the temperature value of \mathbf{d}_j . $\hat{\omega}_{i,j} = 1$ when the following function e is minimized,

$$e = \|\mathbf{m}_i - (\mathbf{R}\mathbf{d}_j + \mathbf{t})\|^2 + K|h_{mi} - h_{dk}|^2, \quad (20)$$

and $\omega_{i,j} = 0$ otherwise.

The above calculation is repeated until the value of $E_T(\mathbf{R}, \mathbf{t})$ converges.

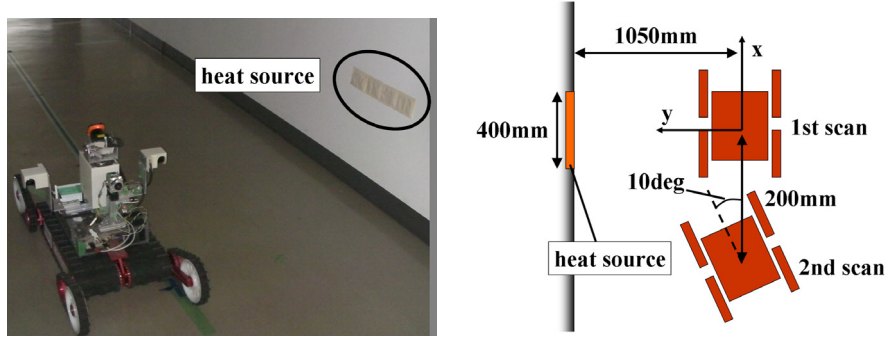


Fig. 9. Experimental scene (left) and parameters of motion (right).

4.4 Simple experiment

To evaluate the proposed thermo ICP matching, we conducted a simple experiment in a corridor environment that has a few geometric features, and compared the results with those of conventional ICP matching. Figure 9 (left) shows the experimental setup. There is a heat source, a disposable body warmer, attached to the corridor wall. In this environment, the robot captured two scan sets. The first scan was conducted at the origin of the world coordinates, and the second scan was conducted at $(x, y, z, yaw) = (-200\text{mm}, 0\text{mm}, 0\text{mm}, 10^\circ)$. Figure 9(right) shows the motion of the robot. Figure 10 shows top view of the results before ICP matching. It can be seen that the two scans do not overlap at all.

First, we applied conventional ICP matching to the data based on Equation (18), and obtained \mathbf{R} and \mathbf{t} . The result in the top view is shown in Fig.11(left), and its zoomed birds-eye-view is shown in Fig.11(right). The method seems to have succeeded in matching two scanned data, in the left figure. However in the right figure, you can see that two colors on the wall are not coincident, and the black circles that represent occluded unscanned areas are completely matched even if the scanned position of the robot was different. The calculated translation vector was $(x, y, z, yaw) = (-13.5\text{mm}, 0.0\text{mm}, -8.2\text{mm}, 10.7^\circ)$, and the value of the x-axis was far from the correct value, -200mm . This is understandable because there were very few features along the x-axis in the corridor.

Second, we applied the proposed Thermo-ICP matching to the data based on Equation (19). The result in the top view is shown in Fig.12(left), and its zoomed birds-eye-view is shown in Fig.12(right). The method succeeded in matching two scanned data. In the right figure, you can see that two colors on the wall are coincident, and the black circles that represent occluded unscanned areas are out of alignment in the amount of robot's translation. The calculated translation vector was $(x, y, z, yaw) = (-181.6\text{mm}, -7.3\text{mm}, -12.0\text{mm}, 11.3^\circ)$. The value of the x-axis was much

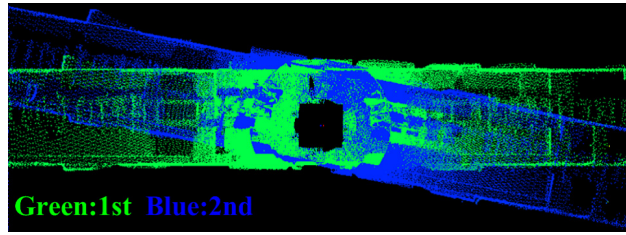


Fig. 10. Before scan matching

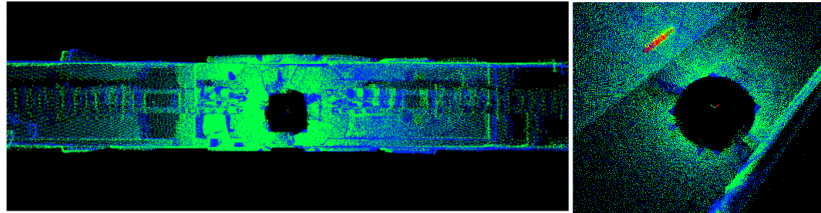


Fig. 11. ICP matching result

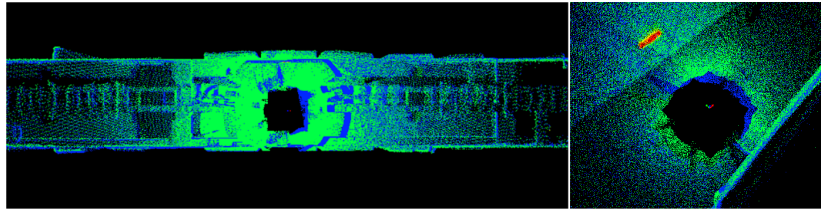


Fig. 12. Thermo ICP matching result

closer to the correct value: -200mm . This is a very simple but clear example that proves the effectiveness of the proposed thermo ICP.

5 Conclusions

In this paper, we introduced a 3D range scanner to obtain a 3D range map and an infrared camera to obtain temperature images; in addition, we proposed a fusion method to integrate the data from both devices to obtain a 3D thermography map. Our system was applied to a simulated disaster environment, and it captured the victims' data successfully. The experiment proved the validity of this method. We then applied the method to the implementation of a Thermo-ICP algorithm, and to a simple experiment. It was a very ad hoc experiment, and we did not apply it in a real environment. However, the result showed the effectiveness of the 3D thermography data for improving matching results. In the future, plan to perform more realistic experiments to confirm the validity of the method.

References

1. Binoy Shah and Howie Choset. Survey on urban search and rescue robots. *Journal of the Robotics Society of Japan*, 22:582–586, 2004.
2. Special issue of advanced robotics: Advanced research and development of robotics for search and rescue. *Journal of Advanced Robotics*, 19(3):219–347, 2005.
3. F.Matsuno and S.Tadokoro. Rescue robots and systems in japan. In *Proceedings of 2004 IEEE International Conference on Robotics and Biomimetics*, pages 12–20, 2004.
4. Keiji Nagatani, Yoshito Okada, Naoki Tokunaga, Kazuya Yoshida, Seiga Kiribayashi, Kazunori Ohno, Eijiro Takeuchi, Satoshi Tadokoro, Hidehisa Akiyama, Itsuki Noda, Tomoaki Yoshida, and Eiji Koyanagi. Multirobot exploration for search and rescue missions: A report on map building in robocuprescue 2009. *Journal of Field Robotics*, 28(3):373–387, 2011.
5. H. Kitano, S. Tadokoro, I. Noda, H. Matsubara, T. Takahashi, A. Shinjou, and S. Shimada. Robocup rescue: Search and rescue in large-scale disasters as a domain for autonomous agents research. In *IEEE International Conference on Systems, Man, and Cybernetics, 1999*, volume 6, pages 739–743. IEEE, 2002.
6. S. Fleck, F.Busch, P.Biber, W.Strasser, and H.Andreasson. Omnidirectional 3d modeling on a mobile robot using graph cuts. In *IEEE International Conference on Robotics and Automation*, pages 1748–1754, 2005.
7. Yunsu Bok, Youngbae Hwang, and In So Kweon. Accurate motion estimation and high-precision 3d reconstruction by sensor fusion. In *IEEE International Conference on Robotics and Automation*, pages 4721–4726, 2007.
8. Keiji NAGATANI, Takayuki Matsuzawa, and Kazuya Yoshida. Scan-point planning and 3-d map building for a 3-d laser range scanner in an outdoor environment. In *Field and Service Robotics*, pages 207–217, 2010.
9. Ivan Grubisic, Luko Gjenero, Tomislav Lipic, Ivan Sovic, and Tibor Skala. Active 3d scanning based 3d thermography system and medical applications. In *MIPRO 2011 Proceedings of the 34th International Convention*, pages 269–273, 2011.
10. S.Lagueta, J.Martinez, J.Armesto, and P.Arias. Energy efficiency studies through 3d laser scanning and thermographic technologies. *Journal of Energy and Buildings*, 43:1216–1221, 2011.
11. K.Ohno, T.Kawahara, and S.Tadokoro. Development of 3d laser scanner for measuring uniform and dense 3d shapes of static objects in dynamic environment. In *Proc. of 2008 IEEE International Conference on Robotics and Biomimetics*, 2008.
12. Z.Zhang. A flexible new technique for camera calibration. *IEEE Transactions on Pattern Analysis and Machine Intelligence*, 22(11):1330–1334, 2000.
13. IHI Corp. Calibration method and instrument for infrared cameras. Japan patent. 2010-48724, 2010.
14. Keiji Nagatani, Naoki Tokunaga, Yoshito Okada, and Kazuya Yoshida. Continuous acquisition of three-dimensional environment information for tracked vehicles on uneven terrain. In *Proceedings of the 2008 IEEE International Workshop on Safety, Security and Rescue Robotics*, pages 25–30, 2008.
15. Paul J. Besl and Neil D. McKay. A method for registration of 3-d shapes. *IEEE Tran. on Pattern Analysis and Machine Intelligence*, 14(2):239–256, 1992.